Supplement of Atmos. Chem. Phys., 22, 14355–14376, 2022
https://doi.org/10.5194/acp-22-14355-2022-supplement


*Supplement of*

# Assimilation of S5P/TROPOMI carbon monoxide data with the global CAMS near-real-time system

**Antje Inness et al.**

*Correspondence to:* Antje Inness (a.inness@ecmwf.int)

## S1 Documentation of CAMS model upgrades and TROPOMI algorithm upgrades (2018-2021)

**Table S1: CAMS model cycles used between November 2018 and December 2021 and changes relevant for CO. The horizontal resolution of the global CAMS model was Tl511 throughout the period. More details about model upgrades can be found on https://confluence.ecmwf.int/display/CKB/CAMS%3A+Global+atmospheric+composition+forecast+data+documentation#CAMS:Globalatmosphericcompositionforecastdatadocumentation-EvolutionoftheCAMSglobalforecastingsystem).**

| In operation from | Model cycle | Model changes affecting CO |
|---|---|---|
| 2018-06-26 | CY45R1 | Using MACCity (anthropogenic) and MEGAN_MACC (biogenic) emissions<br>Super-obbing used with sobmin=1, no separate super-obbing for clear and cloudy data |
| 2019-07-09 | CY46R1 | Vertical resolution change from 60L to 137L, including new background errors for 137L<br>**New emissions inventories**: CAMS_GLOB_ANT v2.1 (anthropogenic) and CAMS_GLOB_BIO v1.1 (biogenic)<br>Biomass-burning injection heights from GFAS used and updated diurnal cycle<br>Online calculation of dry deposition velocities for trace gases<br>Updates to wet deposition parameterisations<br>Updates to chemical reaction rates<br>Super-obbing used with sobmin=6, separate super-obbing for clear and cloudy data |
| 2020-10-06 | CY47R1 | Updated emissions inventories: CAMS_GLOB_ANT v4.2 (anthropogenic)<br>Update to GFASv1.4 biomass-burning emissions<br>Excluded agricultural waste burning from CAMS_GLOB_ANT, avoiding double-counting with GFAS<br>Super-obbing used with sobmin=1, separate super-obbing for clear and cloudy data |
| 2021-05-18 | CY47R2 | None |
| 2021-10-12 | CY47R3 | Updated background error statistics |

**Table S2: TROPOMI algorithm upgrades (from TROPOMI readme file https://sentinels.copernicus.eu/web/sentinel/user-guides/sentinel-5p-tropomi/document-library)**

| In operation from | Processor Version | Relevant improvements of TROPOMI CO retrieval |
|---|---|---|
| 2018-11-22 | 01.02.00 | Adjusted qa_value in case of eclipse |
| 2018-12-05 | 01.02.02 | Sun glint was wrongly considered in the qa_value calculation in previous versions |
| 2019-03-27 | 01.03.00 | Added new variables: eastward_wind and northward_wind |
| 2019-04-30 | 01.03.01 | None |
| 2019-07-03 | 01.03.02 | Offline and NRTI processing chains employ the same algorithm since this Version |
| 2019-08-06 | | TROPOMI resolution upgrade (for SWIR: 7 km x 7 km before, 5.5 km x 7 km after) |
| 2020-12-02 | 01.04.00 | None |
| 2021-07-05 | 02.02.00 | Update $CH_4$, CO and $H_2O$ cross sections in the CO and $CH_4$ processors. CO de-striping algorithm for offline data. Improved L1b v2.0 data products |
| 2021-11-17 | 02.03.01 | None |

## S2 Monitoring of TROPOMI NRT CO data

Figure S1 shows maps of seasonal mean TROPOM CO columns between December 2018 and November 2021. CO values are generally higher in the NH than in the SH, except in the biomass burning regions in the tropics. This reflects the greater anthropogenic emissions in the NH (e.g., Fortems-Cheiney, 2011). Values in the NH are highest during winter and spring, largely due to the lower concentrations of the OH radical during winter, which is the major sink for CO. The largest NH TCCO values are found over southeast Asia in DJF and MAM, and transport of CO rich air from southeast Asia and North America eastwards by the prevailing winds leads to high CO columns over the North Pacific and North Atlantic, respectively. Minimum values in the NH are found in JJA except in areas affected by boreal wildfires (e.g., Siberia, Northern America). CO from biomass burning in the tropics has a different seasonality. In Africa, maximum CO columns are seen north of the equator in DJF, when biomass burning takes place in the Sahel region and equatorial West Africa during the local dry season. In MAM the fire signal over Africa is weaker, and by JJA the affected area has moved south of the equator. In SON the signal is weaker than in JJA but extends further to the south and east. It generally peaks in August, but the season extends to November. In South America the strongest biomass burning signal is seen in SON. Here, deforestation fires and agricultural fires occur south of 10˚S during August–October with a peak in September.

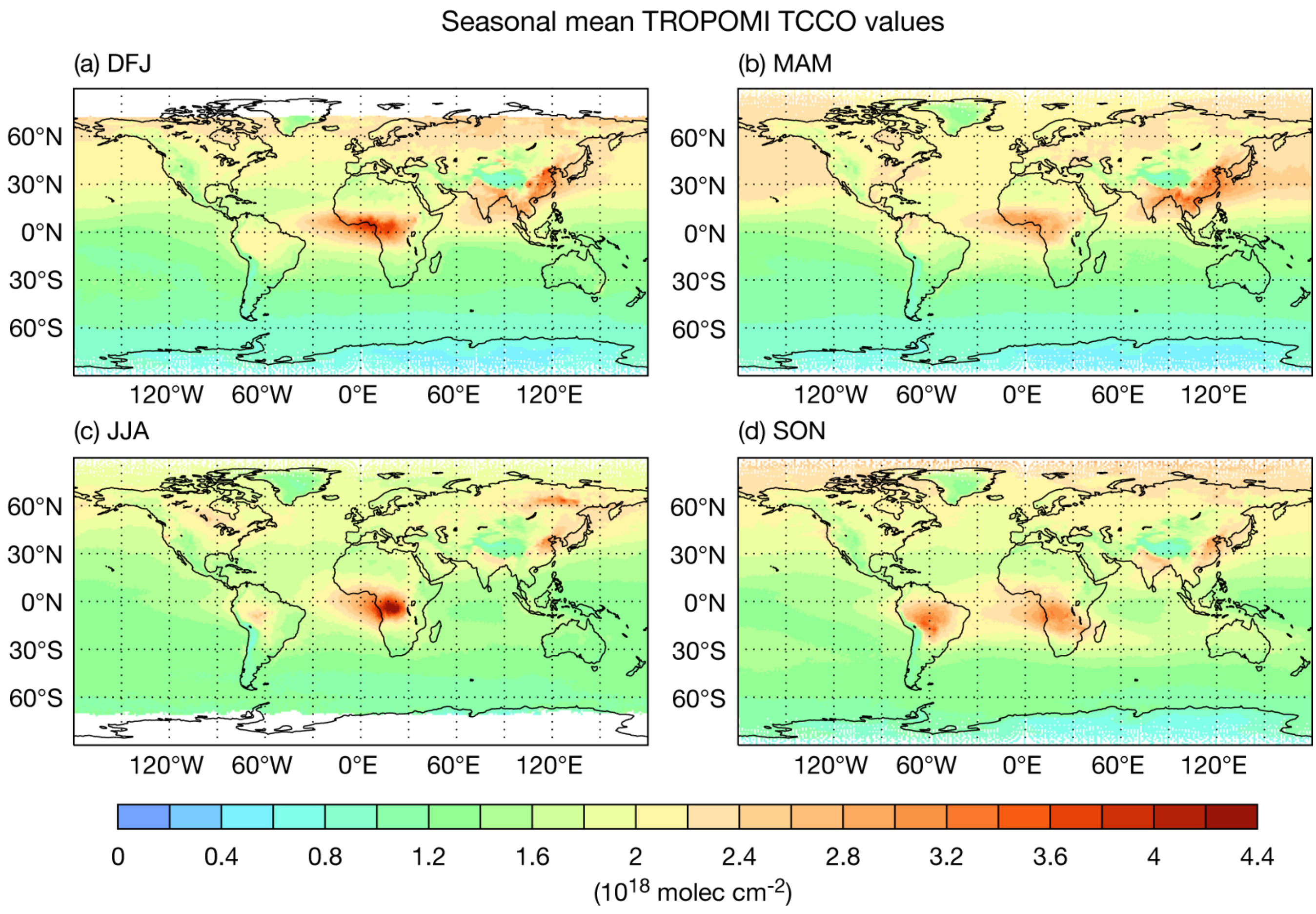


**Figure S1: Maps of seasonal mean TROPOMI CO columns in $10^{18}$ molec/cm$^2$ for (a) DJF, (b) MAM, (c) JJA and (d) SON for the period December 2018 to November 2021. Shown are all 'good' values, i.e., all observations given qa_value >0.5 by the data providers.**

Figure S2 shows the seasonal mean differences between TROPOMI TCCO observation values and CAMS analysis fields. The TROPOMI averaging kernels were applied to the CAMS model profiles in the calculation. The differences are positive everywhere except in a small area over Indonesia in SON, which is affected by biomass burning. The largest absolute differences are found at high latitudes in the NH in DJF, and over SE Asia, as well as over tropical Africa in DJF and JJA. We also see large differences over sea in the area of the South Atlantic Anomaly. These were traced back to observations with qa_value=1 but marked as clear-sky. In these cases, the forward model assumes a cloud free atmosphere which makes no sense over oceans due to the low reflectivity of water in the SWIR. We have excluded these observations in the assimilation experiment discussed in Section 3 of the main paper.

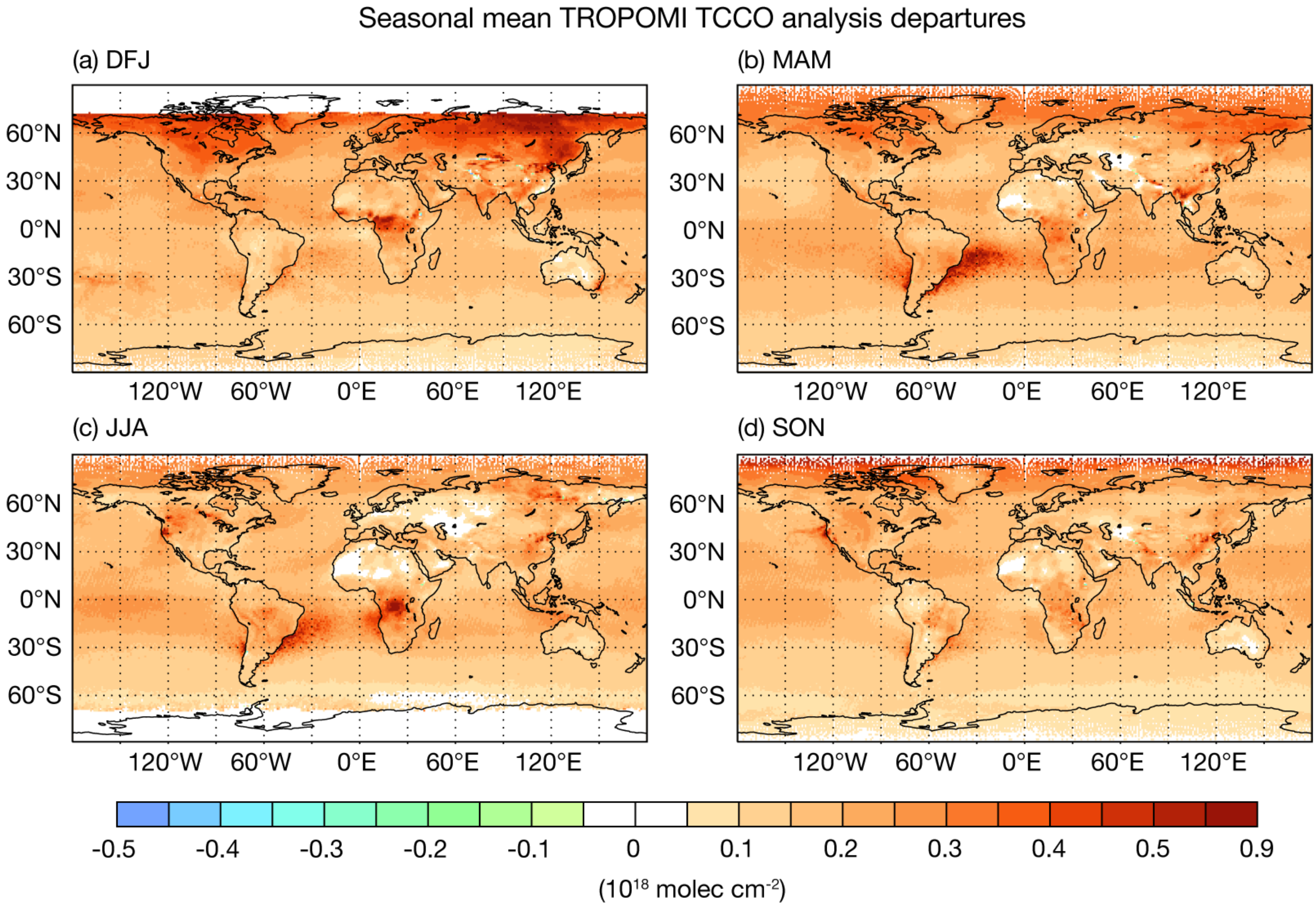


**Figure S2: Seasonal mean maps of TROPOMI CO analysis departures in $10^{18}$ molec/$cm^2$ for (a) DJF, (b) MAM, (c) JJA and (d) SON for the period December 2018 to November 2021. Shown are all 'good' values, i.e., all observations given qa_value>0.5 by the data providers.**

Figure S3 shows boxplots of relative differences between TROPOMI TCCO and CAMS analysis values for the various latitude bands for the period 2018-11-19 to 2021-12-31. Averaged over the globe the median analysis departures are of the order 9-11%, with the smallest departures (median value of 9.4%) seen for cloudy data over land and the largest departures (10.7%) over sea. In the polar latitude bands, i.e., the areas where no satellite data are assimilated in the CAMS system, the analysis departures are largest (11-14%). In NH midlatitude (60-30ºN) the largest departures are found for clear data over land (10.5 %), while cloudy data over land have smaller departures (9.3 %), and the smallest departures in this latitude band is found over sea (8.4 %). In the Tropics the largest analysis departures are found over sea (11.0 %) while values over land have a median of 8.8 % for cloudy observations and 6.6 % for clear-sky observations. In the SH mid-latitudes, the smallest median analysis departures are also found for clear-sky data over land (8.9 %) and the largest ones over sea (10.7 %).

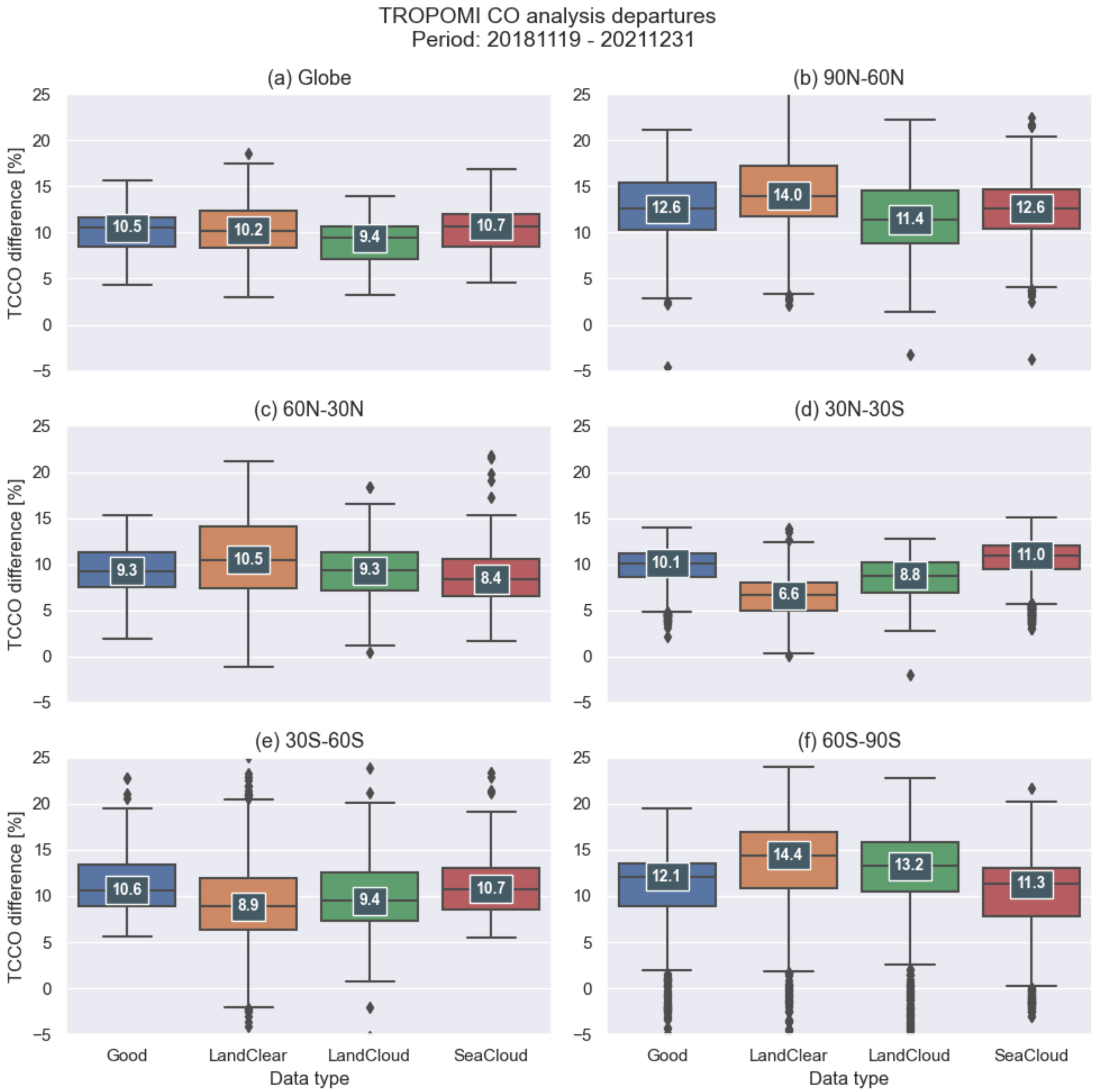


**Figure S3: Boxplot of relative differences between TROPOMI TCCO observation and CAMS values values in % for the period 2018-11-19 to 2021-12-31 and the areas: (a) Globe, (b) 90-60°N, (c) 60-30°N, (d) 30°N-30°S, (e) 30-60°S and (f) 60-90°S. The box extends from the first (Q1) to the third (Q3) quartile values of the data, with a line at the median (Q2). The whiskers extend from the edges of box to show the range of the data. By default, they extend no more than 1.5 * IQR (IQR = Q3 - Q1) from the edges of the box, ending at the farthest data point within that interval. Outliers are plotted as separate dots. 'Good' data are all TROPOMI pixels given qa_values >0.5 by the data providers.**

Figure S4 shows timeseries of the global mean daily analysis departures, observation values, standard deviation of observations and number of observations for TROPOMI TCCO in the NRT CAMS system for the period 2018-11-19 to 2021-12-31. The TROPOMI TCCO data were monitored passively during this period, i.e., not used in the analysis, and therefore have no impact on the CAMS CO fields. The timeseries of the analysis departures is affected by model upgrades (see Table S1) as well as by TROPOMI retrieval algorithm upgrades (see Table S2), while the timeseries of the observations and standard deviation of observations are only affected by changes to the TROPOMI retrieval algorithm. The changes in TROPOMI data numbers in July 2019 and October 2020 seen in Fig. S4 come from changes to the settings for creating the super-observations and not from changes to the TROPOMI NRT data delivery. In the current CAMS configuration (CY47R3, see Table S1), super-observations are created if at least one observation is located in the grid-box. However, due to a coding error, in an early

CAMS configuration (CY46R1), which was operational between 2019-07-09 and 2020-10-05 (see Table S1), super-observations were only created if at least 6 observations were found in a grid-box. This led to a reduced number of super-observations during this period, and particularly affected data at cloud boundaries, where there are often smaller numbers of data of one type in one grid box. In the model cycle used prior to 2019-07-09 (CY45R1) super-observations were created if at least one observation was available in a grid-box, but the super-observation method did not distinguish between clear and cloudy data. This was later corrected. These changes explain the differences in the number of data displayed in Fig. S4, but there is no noticeable impact from this change on the analysis departures and observation values.

A small increase in data numbers is seen in August 2019 when the TROPOMI horizontal resolution was increased from 7 km x 7 km to 5.5 km x 7 km, but this increase is small, because TROPOMI data were already used at a resolution of T511 in the CAMS system. Separate timeseries are shown in Fig. 8 for good data (i.e., all observations with qa_values >0.5), clear and cloudy data over land, and cloudy data over sea. The analysis departures are positive throughout the time period, denoting that TROPOMI TCCO data are always larger than the CAMS analysis values. This agrees with the negative bias of the CAMS CO data that is documented in the routine CAMS evaluation reports (e.g., Errera, et al., 2021). The timeseries show a change to increased departures in July 2019 (from relative differences between 5-10% for 'good' data before July 2019 to 10-15% afterwards). Such an increase is not seen in the observation timeseries and is related to the CAMS model upgrade to CY46R1. This model upgrade included a change to the anthropogenic and biogenic emission data sets used in the CAMS NRT system (from MACCity and MEGAN_MACC prior to July 2019 to CAMS_GLOB_ANT and CAMS_GLOB_BIO afterwards). This change led to lower CAMS CO values and an increased negative bias relative to independent observations, as seen in Fig. 3 of the main paper, and was also reported in the quarterly CAMS evaluation reports on https://atmosphere.copernicus.eu/eqa-reports-global-services (e.g. Errera et al., 2021). The other changes listed in Tables S1 and S2 had smaller impacts on the global TCCO field, but there is a change after the TROPOMI algorithm upgrade in July 2021 leading to lower analysis departures, and after the CAMS upgrade to CY47R3 in October 2021 after which the global mean analysis departures for all observation types are below about 8%. The TROPOMI upgrade in July 2021 included an upgrade to the CO and $CH_4$ cross sections used in the retrieval. It is possible that the better fit of the methane absorption gives better cloud parameters and hence a better estimation of the vertical sensitivity.

The timeseries of the observation values and the departures show clear differences between the TROPOMI observations over land and sea (to be expected as they cover different areas), and also pronounced differences between the clear-sky and cloudy data over land the origin of which is not yet clear. The timeseries of the observation standard deviation shows several spikes during NH summers related to boreal wildfires that emit large amounts of CO into the atmosphere (Witze 2020; https://atmosphere.copernicus.eu/copernicus-reveals-summer-2020s-arctic-wildfires-set-new-emission-records). The spike seen in Fig. S4 in January 2020 is related to large Australian bushfires in 2019/2020 (Li et al., 2020; Ohneiser, 2020; Pope et al., 2021; John et al., 2021; van der Velde et al., 2021).

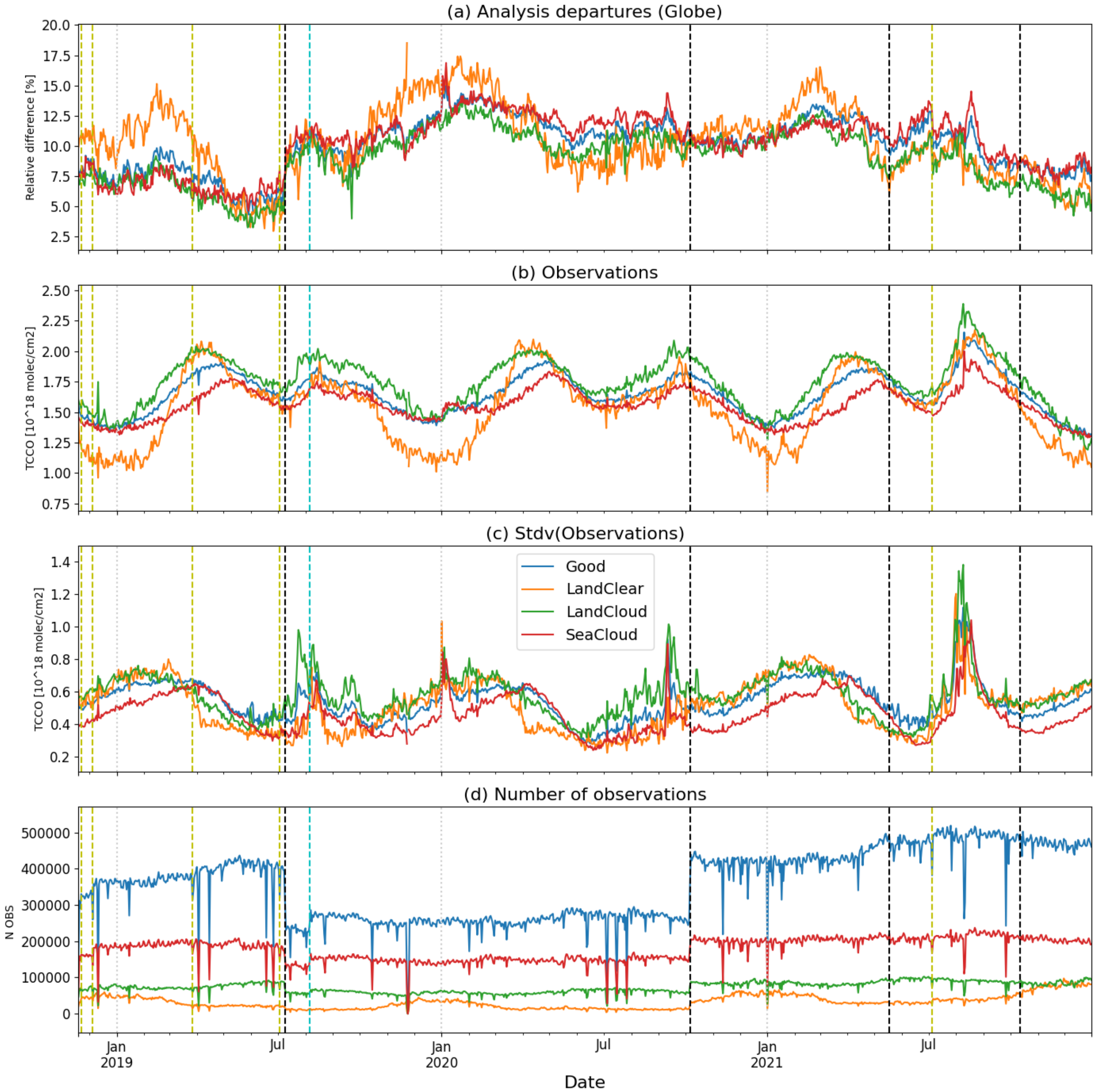


**Figure S4: Timeseries of daily mean global mean TROPOMI TCCO (a) analysis departures (in %), (b) observations (in $10^{18}$ molec/cm$^2$), (c) standard deviation of observations (in $10^{18}$ molec/cm$^2$) and (d) number of observations for the period 2018-11-19 to 2021-12-31. Vertical dashed black lines mark IFS model upgrades (see Table S1), yellow lines TROPOMI algorithm upgrades (see Table S2), the cyan line the TROPOMI horizontal resolution upgrade on 2019-08-06 and the grey dotted lines the year changes.**

As already discussed in Section 2.1 of the main paper, CAMS validation reports show negative biases for tropospheric CO against NDACC FTIR data of about -5 to -15 % after the change to 46R1 in July 2019 and -5 to -10 % against TCCON data, as well as negative biases with respect to MOPITT (-5 to -10 %) and IASI (-10 to -30 %). Figure 3 of the main paper also shows the negative bias in CAMS TCCO after the model upgrade in July 2019 of between -3% to -15% with respect to NDACC FTIR data.

**S3 Boreal wildfires July and August 2021**

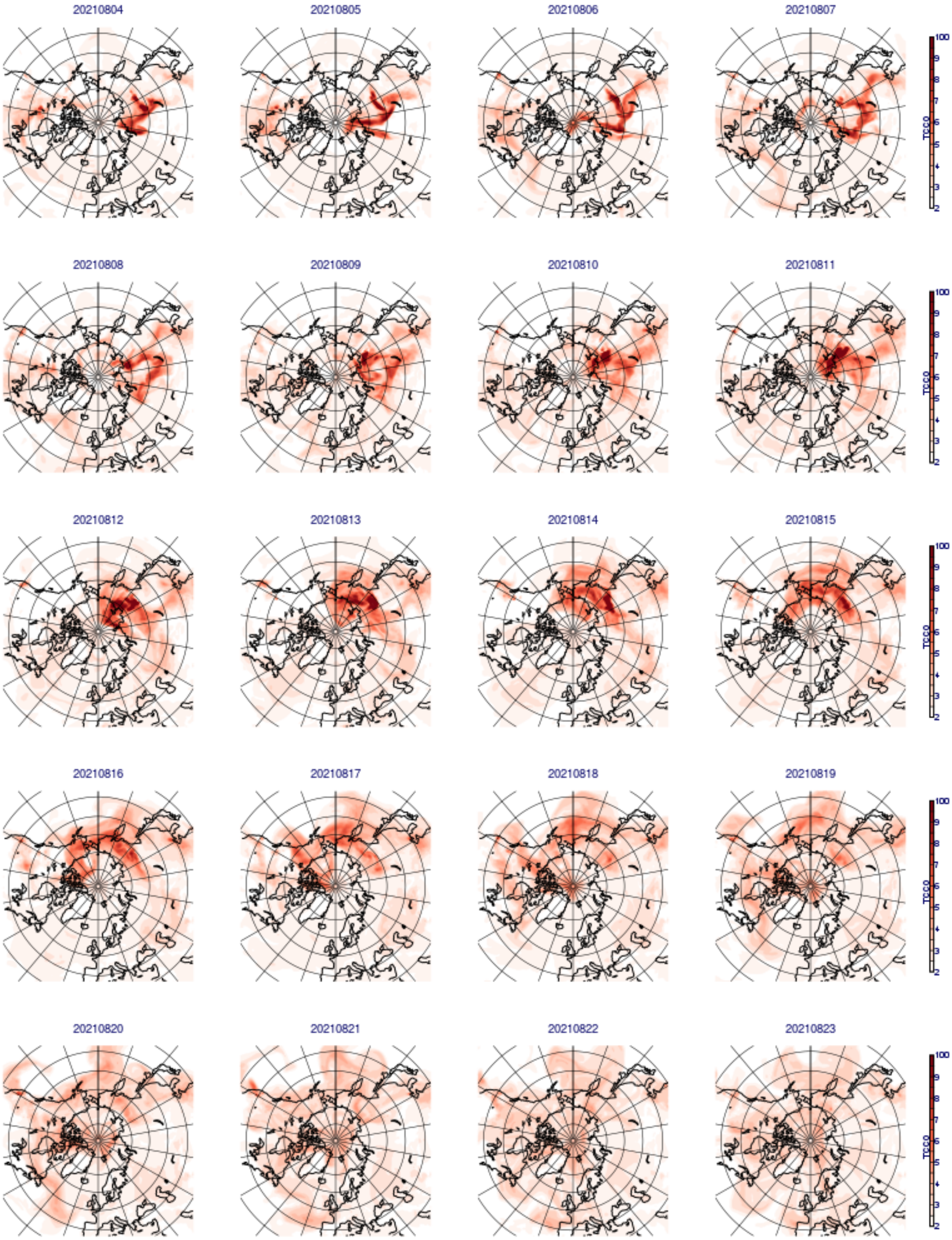


**Figure S5: TCCO fields in $10^{18}$ molec/cm$^2$ from ASSIM for the period 4 to 23 August 2021.**

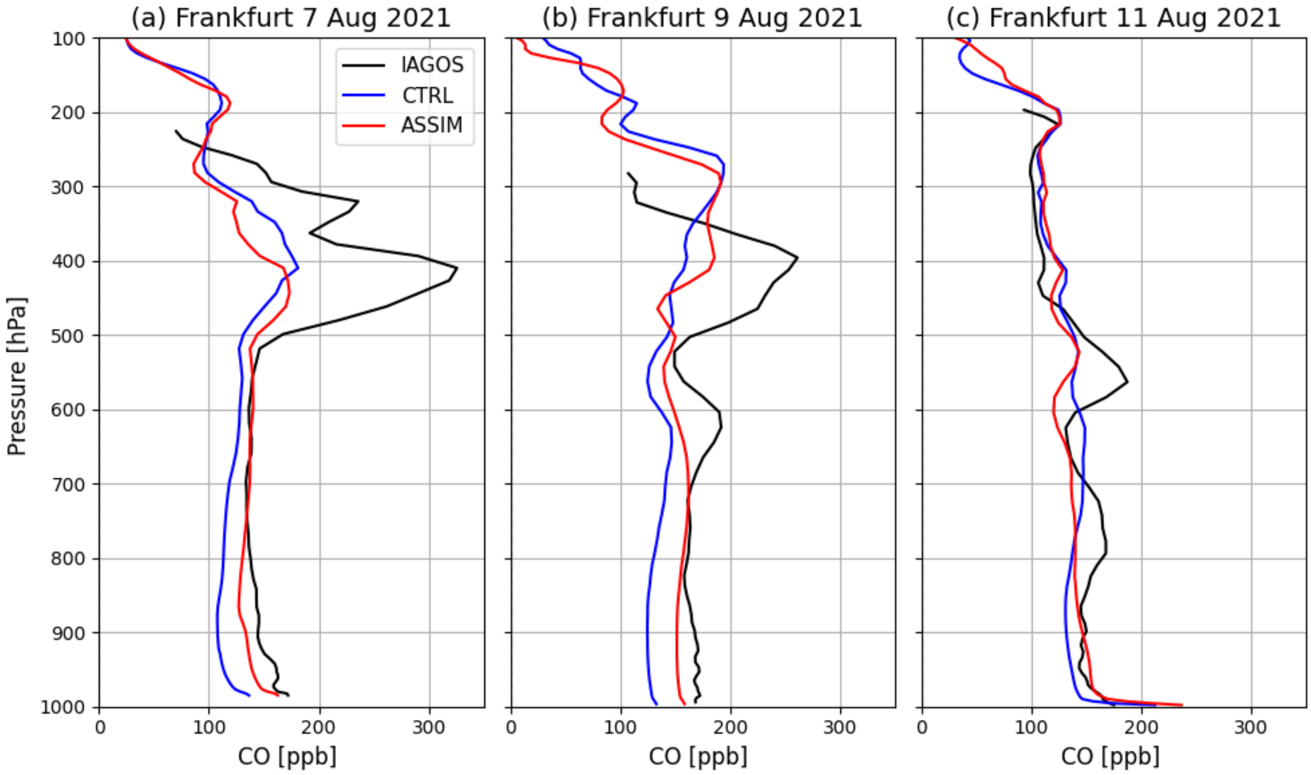


**Figure S6: Like Fig. 16 but at Frankfurt on (a) 7 August, (b) 9 August and (c) 11 August 2021.**

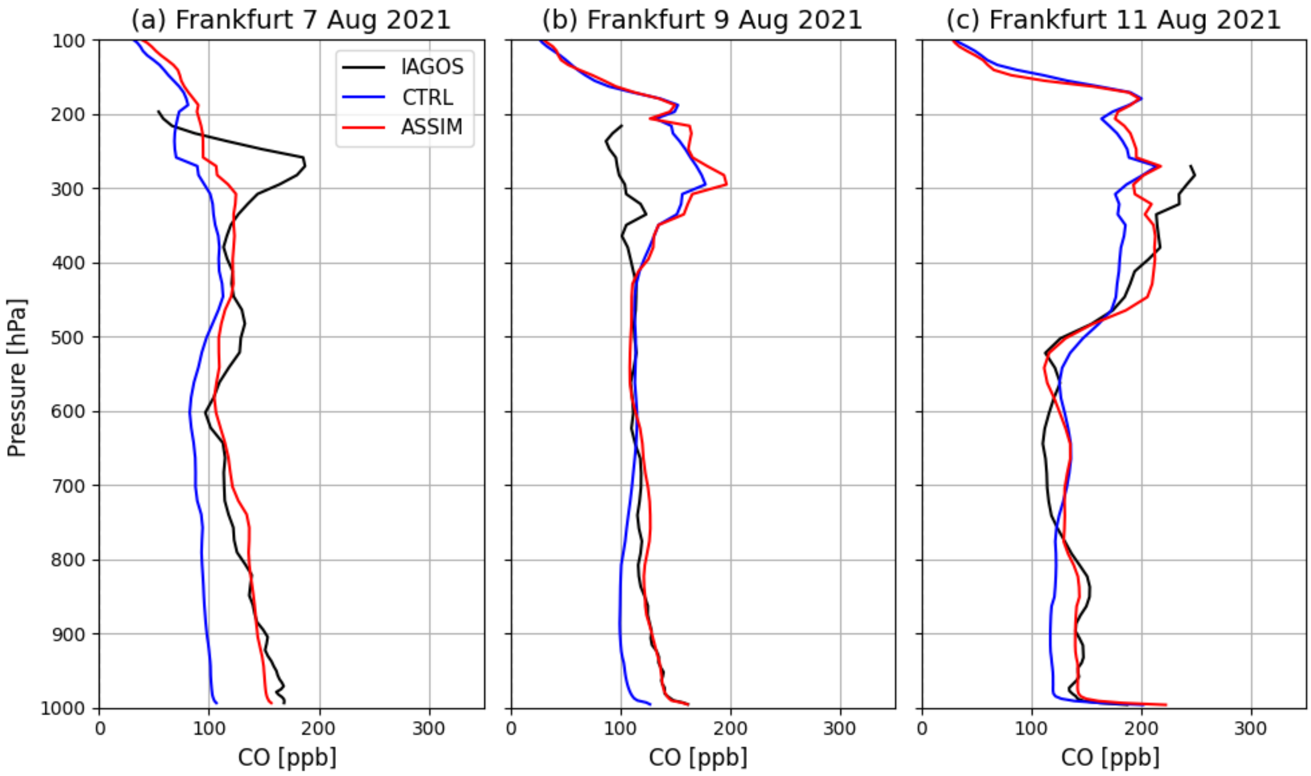


**Figure S7: Like Fig. 16 but at Frankfurt on (a) 19 August, (b) 20 August and (c) 21 August 2021.**

5

## References


John, S. S., Deutscher, N. M., Paton-Walsh, C., Velazco, V. A., Jones, N. B., and Griffith, D. W. T.: "2019–20 Australian Bushfires and Anomalies in Carbon Monoxide Surface and Column Measurements", Atmosphere 12, no. 6: 755, https://doi.org/10.3390/atmos12060755, 2021.

Li, M., Shen, F. & Sun, X.: 2019–2020 Australian bushfire air particulate pollution and impact on the South Pacific Ocean, Sci Rep 11, 12288, https://doi.org/10.1038/s41598-021-91547-y, 2021.

Ohneiser, K., Ansmann, A., Baars, H., Seifert, P., Barja, B., Jimenez, C., Radenz, M., Teisseire, A., Floutsi, A., Haarig, M., Foth, A., Chudnovsky, A., Engelmann, R., Zamorano, F., Bühl, J., and Wandinger, U.: Smoke of extreme Australian bushfires observed in the stratosphere over Punta Arenas, Chile, in January 2020: optical thickness, lidar ratios, and depolarization ratios at 355 and 532 nm, Atmos. Chem. Phys., 20, 8003–8015, https://doi.org/10.5194/acp-20-8003-2020, 2020.

Pope, R. J., Kerridge, B. J., Siddans, R., Latter, B. G., Chipperfield, M. P., Arnold, S. R., Ventress, L. J., Pimlott, M. A., Graham, A. M., Knappett, D. S., and Rigby, R.: Large enhancements in Southern Hemisphere satellite-observed trace gases due to the 2019/2020 Australian wildfires. Journal of Geophysical Research: Atmospheres, 126, e2021JD034892. https://doi.org/10.1029/2021JD034892, 2021.

van der Velde, I.R., van der Werf, G.R., Houweling, S., Maasakkers, J. D., Borsdorff, T., Landgraf, J., Tol, P., van Kempen, T. A., van Hees, A., Hoogeveen, R., Veefkind, J. P., and Aben, I.: Vast $CO_2$ release from Australian fires in 2019–2020 constrained by satellite, Nature 597, 366–369, https://doi.org/10.1038/s41586-021-03712-y, 2021.